AIAA 93-0362

The Strain Exerted by a Vortex on a Flame - Determined from Velocity Field Images

James F. Driscoll[1], D.J. Sutkus[2], Wm. L. Roberts[3], M.E. Post[4], and L. P. Goss[4]

[1]Dept. of Aerospace Engineering, University of Michigan,
[2]Aero Propulsion and Power Lab, Wright-Patterson AFB,
[3]Lockheed Engr. and Sciences Corp., Hampton VA,
[4]Systems Research Laboratories, Dayton OH

31st Aerospace Sciences Meeting & Exhibit
January 11-14, 1993 / Reno, NV

The Strain Exerted by a Vortex on a Flame - Determined from Velocity Field Images

James F. Driscoll[1], D.J. Sutkus[2], Wm. L. Roberts[3], M.E. Post[4], and L. P. Goss[4]

[1]Dept. of Aerospace Engr., Univ. of Michigan, [2] Aero Propulsion and Power Lab., Wright-Patterson AFB, [3]Lockheed Engr. and Sciences Corp., Hampton VA, [4]Systems Research Lab., Dayton OH

Abstract

Velocity field imaging techniques were used to observe how a single toroidal vortex, which represents one eddy in a turbulent flow, exerted aerodynamic strain on a premixed flame. By achieving dense seeding of the flow, the spatial derivatives of velocity were determined accurately, which allowed the following to be measured as a function of space and time: the aerodynamic strain rate tangential to the flame, the rate of flame stretch, the vorticity field, the shear strain rate field and the flow pattern near the forward stagnation point. The vortex strength was sufficient to cause quenching of the flame.

An unexpected result was that the maximum strain on the flame did not occur on the centerline near the forward stagnation point. Instead the strain rate distribution was significantly different from numerical simulations of Poinsot, Veynante and Candel, for which strain is maximum on centerline. The difference is due to the different vortex sizes considered, which indicates that small vortices exert a different strain rate distribution on a flame than larger vortices, and that the process cannot be modelled as being self-similar. During flame quenching, the maximum local strain rate was measured to be 35 sec^{-1}, which is similar to the value of 42 sec^{-1} that is required to quench a steady, planar counterflow flame of the same equivalence ratio.

The velocity field images also show how the flame created vorticity in the products. This flame-generated turbulence resulted from gas expansion and the baroclinic torque term in the vorticity transport equation. The velocity field ahead of the flame also was affected by the flame, but no vorticity was generated in the reactants; this validates the assumption made in many models that the turbulence in the reactants is undisturbed by the flame.

Introduction

The motivation for the present work is the need to better understand the phenomenon known as aerodynamic strain and to develop consistent ways to add aerodynamic strain to models of turbulent flames [1-8]. The effects of strain can be large; for example, as the turbulence level ahead of a premixed flame is increased, the turbulent burning velocity eventually no longer increases; instead the burning velocity eventually decreases to zero and the entire flame is strained out [9]. Strain also steepens the scalar gradients within flames, which enhances preferential diffusion effects and which in turn can cause a two-fold change in the turbulent burning velocity, as reported by Wu, Kwon, Driscoll and Faeth [10].

One promising way to add strain to models of high Reynolds number turbulent flames is to use a thin-interface simulation. With this approach the reaction zone is represented as a thin, wrinkled interface that propagates normal to itself at a local burning velocity that depends on the local aerodynamic strain rate and flame curvature [3-8]. The relation between burning velocity and strain is determined from measurements or calculations performed for a counterflow flame having a known strain rate. The velocity field and resulting strain rate are simulated by either a discrete vortex method or by a stochastic method. The thin-interface simulations to date [3-8] produce instantaneous images of very wrinkled flames that are encouragingly similar to experiment.

In order to develop such turbulent flame models, it is important that the vortices in the numerical simulation behave in a manner that is similar to the way actual vortices behave in the presence of a flame. The present work uses an advanced velocity field imaging technique to measure the strain rate that is exerted on a flame during a flame-vortex interaction. Previous papers describe how the apparatus used in the

present work was used to visualize flame wrinkling [11] and flame quenching [12,13] by a vortex. The measurements herein relate the local strain rate on the flame to the global strain rate, as defined below, during the quenching process. The results also will allow for future comparisons of certain scalar profiles, such as profiles of OH concentration and temperature, in this unsteady, wrinkled, strained flame to the profiles calculated for steady, planar, counterflow flames at the same local strain rate, in order to determine if the flame can be modelled as a strained laminar flame as turbulent flow conditions are approached.

The geometry of the flame-vortex interaction that is studied is shown in Fig. 1. A laminar premixed flame propagates upward and the toriodal vortex has a downward convective velocity (U_C). The convective velocity is partially self-induced and partially due to the momentum imparted during vortex creation. Therefore, in the vortex frame of reference the hot products below the vortex in Fig. 1 have a relative velocity of magnitude U_C that is upward, which creates a forward stagnation point below the flame. The velocity components in the x and y directions defined in Fig.1 are u and v, respectively, while u_T is the velocity component that is tangential to the flame surface. The coordinate that is tangential to the flame surface is denoted s. The quantities of interest include the stretch rate K, which is defined as (1/A)dA/dt, where A is the flame sheet area; analysis has shown [14,15] that the contribution to the stretch rate from the velocity components in the two-dimensional plane shown in Fig. 1 is:

$$K_{2D} = \partial u_T/\partial s - S_L/R \qquad (1)$$

where S_L is the laminar burning velocity and R is the local radius of curvature of the flame. The first term in Eq. 1 represents the aerodynamic tangential strain rate on the flame which is denoted S_{tt}. The second term is the rate of area increase due to flame curvature. Also of interest is the normal strain rate S_{xx} , the shear strain rate S_{xy}, and the vorticity component in the z direction ω_z which are :

$$S_{xx} = \partial u/\partial x \quad S_{xy} = (1/2)\,(\partial u/\partial y + \partial v/\partial x)$$
$$\omega_z = \partial v/x - \partial u/\partial y \qquad (2)$$

Simple formulas for the quantities S_{tt}, S_{xx}, S_{xy}, and ω_z can be obtained for the theoretical example of two potential vortices, of circulation $+\Gamma$ and $-\Gamma$ respectively, that are separated by a distance 2a, as shown in Figure 1. Far ahead of the vortex the freestream velocity is U_C. This theoretical example does not include several physical processes of importance, however because of the simplicity of the formulas, it provides a useful comparison to the measurements discussed below. For this theoretical example the velocity and strain fields are:

$$u = -(\Gamma/(2\pi))\,[(y+a)(x^2+(y+a)^2)^{-1} - (y-a)(x^2+(y-a)^2)^{-1}] + U_C \qquad (3a)$$

$$v = -(\Gamma/(2\pi))\,[-x(x^2+(y+a)^2)^{-1} + x(x^2+(y-a)^2)^{-1}] \qquad (3b)$$

$$S_{xy} = (\Gamma/(2\pi))\,[((y-a)^2-x^2)(x^2+(y-a)^2)^{-2} - ((y+a)^2-x^2)(x^2+(y+a)^2)^{-2}] \qquad (4)$$

$$S_{xx} = -S_{yy} = (\Gamma/\pi)\,[-(y-a)x(x^2+(y-a)^2)^{-2} + (y+a)x(x^2+(y+a)^2)^{-2}]$$

During the earliest phase of the interaction, the flame surface, in general, can be represented as a horizontal plane located a distance L below the vortex shown in Fig.1. The tangential strain rate S_{tt} equals $\partial v/\partial y$ and differentiation of Eq. 3b, for x equal to -L, yields:

$$S_{tt}(\text{planar flame}) = (\Gamma L/\pi)\,\{((y+a)[L^2+(y+a)^2]^{-2} - (y-a)[L^2+(y-a)^2]^{-2}\} \qquad (5)$$

Therefore, the tangential strain rate S_{tt} is distributed along a planar flame as shown in Figure 1b, which was calculated using Eq. 5. The strain is seen to reach a maximum on centerline for the planar flame. The planar flame case represents the initial phase of a flame-vortex interaction; this strain distribution also represents an interaction involving a weak vortex, since a vortex with a relatively small rotational velocity will not distort the flame significantly from its initially planar geometry.

For the case of a strong vortex, the flame surface is best represented by the circle of radius R that is shown in Figure 1a. The calculation of the strain rate is straightforward because the tangential velocity u_T is simply the azimuthal velocity ((xv/R)-(yu/R)). S_{tt} is the derivative of u_T with respect to y, multiplied by dy/ds, where the derivative of the tangential coordinate along the interface (ds) is Rdθ. Since y equals Rsinθ, differentiation shows that ds is $R(R^2-y^2)^{-1/2}dy$. It follows that along a circular flame interface the tangential velocity and strain rates are:

$$u_T = (\Gamma/(2\pi R))\,[(R^2-ay)(R^2+a^2-2ay)^{-1} - (R^2+ay)(R^2+a^2+2ay)^{-1}] + U_C y/R \qquad (6)$$

$$S_{tt}(\text{circular flame}) =$$

$$\Gamma/(2\pi)[(a/R^2)(R^2-a^2)]\,(R^2-y^2)^{1/2}\,[(R^2+a^2-2ay)^{-2}+(R^2+a^2+2ay)^{-2}] + (U_C/R^2)(R^2-y^2)^{1/2} \qquad (7)$$

The tangential velocity u_Γ and the tangential strain rate S_{tt} given by Eq. 7 are plotted in Figure 1b for values of Γ, a , R and U_C equal to 524 cm^2/s, 1 cm, 2 cm and zero respectively.

The observation that immediately follows from Figure 1b is that the tangential strain exerted on the flame is highly dependent on how the flame is distorted; the portion of the flame that happens to be located closest to a vortex center will experience the largest strain rate. Therefore the strain is especially sensitive to the flame structure, the vortex structure, and the relative distances between the flame and the vortex. It is believed that models of turbulent flames that correctly simulate the instantaneous flame surface have the potential to incorporate the correct strain effects, which is a major advantage over time-averaged models.

Experimental Arrangement

Two-color particle imaging velocimetry (PIV) diagnostics that were developed by Goss, Post, Trump and Sarka [16] were applied to the flame-vortex experiment developed by Roberts and Driscoll [11]. The experimental apparatus consists of an 11.4 cm x 11.4 cm x 61cm rectangular chamber with a loudspeaker and orifice plate on the top surface and a spark plug on the lower surface. The chamber is filled with a methane-air mixture at an equivalence ratio of 0.55; the loudspeaker is pulsed to create a toroidal vortex which moves downward and the spark ignites a flame which propagates upward. While many vortex sizes, vortex strengths and flame speeds have been studied in our previous work [13], all of the velocity field imaging reported herein was conducted with a single vortex having a toroid diameter (D) of 3.81 cm and a vortex core diameter (d_C) of 0.76 cm. The maximum rotational velocity of the vortex (U_θ) was measured to be 107 cm/s using a laser velocimeter [11]. This velocity occurs at the edge of the vortex core which is defined as the region where the rotational velocity increases linearly with radial distance from the vortex center. Therefore the global strain rate associated with this vortex (U_θ/D) is 28 sec^{-1}. The laminar burning velocity of the flame was measured to be 7.5 cm/sec; this is the difference between the velocity of the flame in the laboratory coordinates (36.5 cm/sec) and the velocity of gas in front of the flame (29 cm/s) on centerline. The former was determined from the flame transit time between two thin filament pyrometers and the latter was determined from the PIV images. A similar laminar burning velocity was measured for these conditions using a video camera and a laser velocimeter [13]. All times that are reported are referenced to the time when the vortex core is a distance 2D from the flame, which defines the beginning of the interaction.

The two-color PIV system developed by Goss and Post [16] uses a frequency doubled Nd:YAG laser to create a green laser light sheet at 532 nm and a second Nd:YAG laser, which pumps a dye laser, to form a red laser light sheet at 640 nm. Laser energy is 20mJ/pulse; each laser sheet has a height of 25 cm and a thickness of 0.1 cm. The experiment is seeded with alumina microballoon particles having a mean diameter of six microns. The green laser sheet is pulsed one millisecond before the red laser sheet and the positions of the particles within a typical 8 cm by 6 cm field of view are recorded on 35 mm color film. Therefore a typical maximum particle velocity of 100 cm/s results in a particle displacement of 1 mm. Directional ambiguity is eliminated with the two-color system because each particle that appears green (which is denoted a "green particle") is imaged at an earlier time than the corresponding red particle. Both light sheets were forced to overlap in space by using a dichroic mirror and the same cylindrical optics. Customized electronics were required to pulse each laser on demand, since the lasers normally operate at fixed repetition rates. Kodak Gold 400 film was used because it has a resolution of 300 line pairs/mm, thus it is able to resolve a 6 micron particle separation with one-to-one imaging. Each color photograph was digitized using an Imapro QCS-35 digital scanner which was hooked to an Apple Macintosh IIfx computer.

The present PIV system uses an efficient three-step algorithm to determine the velocity vector field from a digitized PIV image. The first step is to determine the locations of red and green particles on the digitized image. This is accomplished by use of an algorithm which applies red and green filters to the digitized image and finds particles based on relative pixel intensity counts. The second step is to determine the most probable vector displacement in each 5 mm by 5 mm section of the image by use of the spatial cross-correlation function, which is defined as:

$$c(\xi,\eta) = \Sigma_x\ \Sigma_y\ g(x,y)\ r\ (x-\xi,\ y-\eta) \qquad (8)$$

where g and r represent the coordinates of each green particle and red particle respectively. The correlation function c will have a maximum value in the ξ,η plane and the vector drawn from the origin to this maximum represents the most probable vector displacement in that 5 mm by 5 mm section. The third step is to use a tracking algorithm to pair up the individual red and green particles. For each green particle considered, the

tail of a probable displacement vector is placed at the green particle position. This probable displacement vector is determined by a spatially weighted average of the most probable displacement vectors associated with the three sections closest to the green particle. Near the head of the vector a search is conducted for the nearest red particle. A small search window is opened and the window size is increased, typically to be no more than 10% of the vector length, until a red particle is identified. If no red particle is identified in the window, no velocity vector is associated with that particular green particle. The tracker algorithm is efficient, requiring less than 30 seconds to process the digitized image. A typical image of the velocity field is shown in Figure 2a. The density of valid particle pairs is typically 100 per square cm of the image.

One problem that was encountered was that particles were not observed in the vortex core region, as is seen in Figure 2a. The vortex core is made up of fluid that originated in the wall boundary layer near the orifice plate and was forced out through the orifice. The chamber above the orifice plate was heavily seeded by passing the incoming fuel-air mixture through two separate seeders; one seeded flow entered the chamber below the orifice and one entered above the orifice. However, centrifugal forces or perhaps electrostatic attraction of particles to the orifice wall resulted in insufficient seeding of the vortex cores. Fortunately, for the strong vortex considered, the flame is quenched before it enters the vortex core so the seeding of the vortex cores is not a significant problem. Another problem was that particles acquired a static charge and adhered to the windows, which obscured the view of the camera. A commercial anti-static fabric softener was applied to the windows to solve the problem.

Results

For the case of the vortex alone, with no flame present, the velocity field is shown in Figure 2a. The velocity vectors are in the vortex frame of reference in this figure. To represent the vectors in the lab frame of reference, a downward-pointing vector of magnitude 33.5 cm/s must be added to each vector. Solid lines have been added to identify the forward and rear stagnation points; the flowfield about the vortex with its convective downward velocity is observed to be similar to the laminar flow about a sphere.

Figure 2b shows the flame alone, with velocity vectors represented in the laboratory frame of reference. The flame acts like a piston and forces the fluid ahead of it to move upward at a velocity of 29 cm/s on centerline, as seen in Figure 2b, while the flame itself moves upward at 36.5 cm/s. It is seen that the flame does not disturb the gas that is more than 2 cm ahead of the flame. In the 2 cm region ahead of the flame, the flame does create velocity gradients; but it is shown below that these induced velocity gradients are such that no vorticity is created in the reactants. Figure 2b also shows that there is a rotational motion set up in the product gases below the flame; it is shown below that this motion is associated with vorticity produced by the flame.

Figure 3 shows the flame-vortex interaction at a time of 26 milliseconds where time zero is defined above; this point in the interaction is denoted the intermediate phase. The flame position is defined as the boundary in the PIV photograph were an abrupt change in the particle number density occurs due to gas expansion. This boundary is more distinct in the photograph than in the final velocity images because the photograph contains many small particles that are too small to yield valid velocity vectors; the photograph is similar to an image of Mie scattering from oil drops, which is a common method used to accurately identify the flame surface. The other lines drawn in Figure 3 represent the stagnation point streamlines.

Figure 3 indicates that the flame exists on the reactant-flow side of the stagnation point, as expected. Counterflow flame calculations [17] indicate that the flame can be forced to cross to the opposite side of the stagnation point, but only for extremely large, unrealistic strain rates. It also is observed that the flame curvature is such that the curvature reduces the strain on the flame. It can be observed in Figure 3 that the velocity vectors are all nearly normal to the flame in the region near the centerline. Below the flame, near the forward stagnation point, the velocity vectors are rapidly turned away from the centerline. The velocity field at the late stage of the interaction (t = 34 milliseconds) is shown in Fig. 4.

The velocity tangential to the flame surface (u_T) was determined by use of a computer algorithm. A flame contour approximation was defined in the algorithm by a polynomial fit of flame contour points that were chosen by eye from the original PIV photograph. Velocities at various points on the flame contour were determined by spatially averaging PIV velocity vectors. These spatially averaged velocities were then transformed to a coordinate system having one axis tangential to the approximate flame contour at the point of interest. The velocity component along this axis was defined as u_T. Tangential velocities u_T are shown in Figure 5 for the two different interaction times. The consistent trends observed in Figure 5 indicate that there is sufficient spatial resolution in the measuring technique to resolve u_T from the raw data.

The tangential strain rate S_{tt}, which is $\partial u_T/\partial s$, was determined from the slope of Figure 5 and was added to the curvature term in Eq. 1 to yield the total stretch rate K which is plotted in Figure 6. The curvature term is approximately -2 sec^{-1} over most of the flame, which represents a 6% contribution where the strain rate is maximum. The measured stretch rates display the same trend as the theoretical strain rates shown in Figure 1 that were calculated using Eq. 7 for the theoretical example discussed previously. Near the centerline the strain rates are small because the flame must remain relatively far from the vortex cores, due to the large counterflow velocity directed toward the flame on centerline. At other locations the flame can propagate closer to the vortex cores and the strain rate reaches a local maximum. Poinsot, et al. [18] calculated the strain exerted by a vortex of smaller diameter, normalized by the flame thickness, than used herein. Their maximum strain occured on the centerline, because the smaller vortex did not distort the flame as severely as in the present experiment; for smaller flame distortions, the strain rate profile should correspond more closely to the profile in Figure 1 that is maximum on centerline.

The conditions at which the flame is quenched is a sensitive measure of the chemistry-strain interaction. The maximum stretch rate on the flame just prior to quenching is seen in Figure 6 to be 35 sec^{-1} (quenching occurs at a time of 39 msec, as deduced from previous OH images [13]). This value of stretch is similar to the measured value of 42 sec^{-1} that is required to quench a steady, planar counterflow flame having the same methane-air stoichiometry [13]. This agreement is encouraging evidence that there are similarities between a planar, steady strained flame and a time-varying, wrinkled flame for the same local stretch rate. It is still not conclusively known if the properties of a turbulent flame can be modelled by using the profiles that are calculated for a counterflow flame, since unsteady effects may be important and local flame properties may depend on more than one parameter (ie., stretch). However, using the known counterflow stretch rate at extinction (of 42 sec^{-1}) would correctly predict the observed quenching process in the present study.

The vorticity field was deduced by evaluating $\partial v/\partial x - \partial u/\partial y$ and several contours are shown in Figures 7 and 8. The largest measured vorticity of 30 sec^{-1} occurs at a distance of 0.9 cm from the vortex center. Larger values of vorticity will occur near the vortex core boundary, which is 0.4 cm from the vortex center, however it was not possible to measure vorticity near the vortex cores because of insufficient seeding. The maximum vorticity is estimated to be 2 U_θ/r_c, which is 450 sec^{-1}, since the core has a solid body rotation. Laser velocimetry previously was used to show that U_θ and r_c are 107cm/s and 0.4 cm respectively; the sub-micron oil drops that were used were small enough to uniformly seed the vortex cores. The large difference between measured vorticity at r =0.9 cm and the expected vorticity at r = 0.4 cm is not surprising; for a Rankine vortex (having solid body core rotation surrounded by a potential vortex) the vorticity suddenly decreases from a constant value to zero at the core boundary.

Another observation that was made is that vorticity is generated by the flame, as shown by Figure 7. The flame-generated vorticity results from the flame curvature and is seen to be positive in the products on the left side of the flame and is negative on the right side. Flame curvature arises because of two factors: buoyancy forces [20] and the reduction in burning velocity near the non-adiabatic walls. The only possible sources of vorticity in the flowfield, away from the walls, are given by the four terms in vorticity transport equation:

$$D\omega/Dt = \omega\cdot\nabla v - \omega\nabla\cdot v + \nu\nabla^2\omega + (\nabla\rho\times\nabla p)/\rho^2 \qquad (7)$$

The $\omega\cdot\nabla v$ term is due to vortex stretching and is zero for the axisymmetric conditions considered herein. The diffusion term $\nu\nabla^2\omega$ redistributes the vorticity but cannot cause any net change in the vorticity . The $\omega\nabla\cdot v$ term represents vorticity that is created as the gas expands due to heat release. The baroclinic torque term $((\nabla\rho\times\nabla p)/\rho^2)$ does create vorticity that is of the same sign as the flame generated vorticity observed in Figure 7. The $\nabla\rho$ vector points toward the reactants and the pressure gradient vector ∇p results from gravitational forces and points downward. Thus the cross product results in negative vorticity behind the right hand side of the flame, which causes the clockwise rotation of the velocity vectors observed in Figure 2. From a physical standpoint, a square fluid element can be placed on the flame surface to the right of centerline; the pressure force due to buoyancy acts vertically upward on the center of pressure, which is located at the center of the square element. The center of mass is in the reactant half of the element, so the net torque about the center of mass is clockwise.

The vorticity field at two different times during the flame-vortex interaction is shown in Figure 8. The vortex remains sufficiently strong so that it prevents the flame from propagating over the vortex core where most of the vorticity is located during the time interval considered. Therefore no appreciable decrease in the net circulation can be deduced. Ashurst and McMurtry [21] have used a discrete vortex simulation to evaluate each of the terms in the vorticity transport equation for a

flame-vortex interaction. They found that a flame will generate vorticity that is of the same sign as the incident vorticity at some locations and will generate vorticity of opposite sign at other locations; they concluded that their simulated flame-generated vorticity is a reasonable explanation for the flame-generated vorticity measured by Driscoll and Gulati [22].

To complete the description of the strain field, the shear strain rate S_{xy}, which is $(\partial u/\partial y + \partial v/\partial x)/2$, was determined. Contours appear in Figure 9. The measured contours for the vortex only (Figure 9b) and for the flame and vortex (Figure 9c) are similar to those of a theoretical Rankine vortex. The shear strain contours have eight lobed-shaped regions, four of which have positive shear. Measurements of shear strain in a turbulent flowfield can be of benefit because they allow the determination of the principle axes of the strain field [23], which are rotated from the x,y axes by the angle 0.5 arctan $(2S_{xy}/(S_{xx}-S_{yy}))$. There is evidence that a turbulent flame aligns itself with the principle axes of strain [24].

Conclusions

1. The distributions of the tangential strain rate $\partial u_T/\partial s$ and the stretch rate K have been directly measured along a distorted premixed flame contour, as the flame interacts with a vortex, using velocity field imaging techniques

2. The tangential strain rate is not a maximum on centerline because the velocity field prevents the flame from propagating to a location that is close to the vortex core. Instead, the maximum strain occurs at a location where the distorted flame is able to propagate to a location close to the vortex core, where the velocity gradients are largest.

3. The strain rate distribution on the flame for a smaller vortex, as calculated by direct numerical simulations, is maximum on centerline and differs significantly from the present measurements. It follows that the strain rate distribution on a flame cannot be modelled as a self-similar process but is dependent on the vortex size.

4. The maximum local strain rate also increases with residence time because portions of the flame continue to propagate closer to the high-strain vortex core region.

5. The flame quenches when the maximum local stretch rate is measured to be 35 sec^{-1}, which is similar to the measured stretch rate of 42 sec^{-1} that quenches a steady, planar counterflow flame of similar stoichiometry. It is concluded that unsteady strain effects do not have a major effect on quenching, at least for the conditions of the present experiment.

6. Velocity field images show that the flame generates vorticity due to the action of a baroclinic torque.

Acknowledgements

The measurements were performed at Wright-Patterson AFB in the laboratory that is under the direction of Dr. C.M. Roquemore, whose support and encouragement is appreciated. D. Trump and B. Sarka were instrumental in the development of the PIV diagnostics.

REFERENCES

1. Meneveau, C., and Poinsot, T. (1991). Combust. Flame 86: 311-332.

2. Cant, R.,S., Pope, S.B., and Bray, K.N.C. (1990). Twenty-Third Symposium (International) on Combustion, The Combustion Institute, Pittsburgh, pp.809-815.

3. Ashurst, W.T.(1987). "Vortex Simulation of Unsteady Wrinkled Laminar Flames", Combust. Sci. Technol. 52:325.

4. Wu, M.S., Kwon, S., Driscoll, J.F., and Faeth, G.M.(1992). Comb. Sci.and Technol. 83: 187-202 .

5. Kwon, S., Wu, M.S., Driscoll, J.F., and Faeth, G.M. (1992). Combust. Flame 88: 221-238 .

6. Wu, M.-S., and Driscoll, J.F. (1993) Combust. Flame, to appear.

7. Kerstein, A.R. Ashurst, W.T., and Williams, F.A.(1988) Phys. Rev. A: 37:2728-2731.

8. Lee, T.W. and Santavicca, D.A.(1993) "Flame Front Geometry and Stretch During Interactions of Premixed Flames With Vorticies", to appear, Combust. Sci. Technol.

9. Abdel-Gayed, R.G., Bradley, D., Hamid, N.M., and Lawes, M. (1984). "Lewis Number Effect on Turbulent Burning Velocity", Twentieth Symposium (International) on Combustion, The Combustion Institute, Pittsburgh, p. 505.

10. Wu, M.S., Kwon, S., Driscoll, J.F., and Faeth, G.M.(1991). "Preferential Diffusion Effects on the Surface Structure of Turbulent Premixed Hydrogen-Air Flames" Comb. Sci. Technol. 83: 187-202 .

11. Roberts, W.L. and Driscoll, J.F., Combust. Flame, 87: 245-256 (1991).

12. Roberts, W.L., Driscoll, J.F., Drake, M.C., and Ratcliffe, J.W. (1992).Twenty-Fourth Symposium (International) on Combustion, The Combustion Institute, Pittsburgh, to appear.

13. Roberts, W.L., Driscoll, J.F., Drake, M.C. and Goss, L.P. (1993) "Images of the Quenching of a Flame by a Vortex-To Quantify Regimes of Turbulent Combustion", submitted to Comb. and Flame.

14. Law, C.K., Twenty-Second Symposium (International) on Combustion, The Combustion Institute, Pittsburgh, 1988, pp. 1381-1402.

15. Candel, S.M. and Poinsot, T.J. (1990) "Flame Stretch and the Balance Euqation for the Flame Area", Combust. Sci. Technol. 70:1-15.

16. Goss, L.P., Post, M.E., Trump, D.D. and Sarka, B. (1991). "Two Color Particle Imaging Velocimetry", J. Laser Applic., Winter 1991, pp. 36-42.

17. Darabiha, N., Candel, S.M., and Marble, F.E. (1986). "The Effect of Strain Rate on a Premixed Laminar Flame", Combust. Flame 64: 203-217.

18. Poinsot, T., Veynante, D., and Candel, S. (1990). Twenty-Third Symposium (International) on Combustion, The Combustion Institute, Pittsburgh, pp. 613-619.

19. Poinsot, T., Veynante, D., and Candel, S., J. Fluid Mech. 228: 561-606 (1991).

20. Pelce-Savorin, C., Quinard, J. and Searby, G. (1988). "The Flow Field of a Curved Flame Propagating Freely Upwards", Combust. Sci. Technol. 58: 337-346.

21. Ashurst, W.T. and McMurtry, P.A. (1989). "Flame Generation of Vorticity: Vortex Dipoles from Monopoles", Combust. Sci. Technol. 66: 17-37.

22. Driscoll, J.F. and Gulati, A. (1986). "Measurement of Various Terms in the Turbulent Kinetic Energy Balance Within a Flame and Comparison with Theory", Combust. Flame 72:131-152.

23. Beer, F.P., and Johnston, E.R., Mechanics of Materials, McGraw Hill, NY, 1981.

24. Haworth, D.C. and Poinsot, T.J. (1992). "Numerical Simulations of Lewis Number Effects in Turbulent Premixed Flames", J. Fluid Mech. 244:405-436.

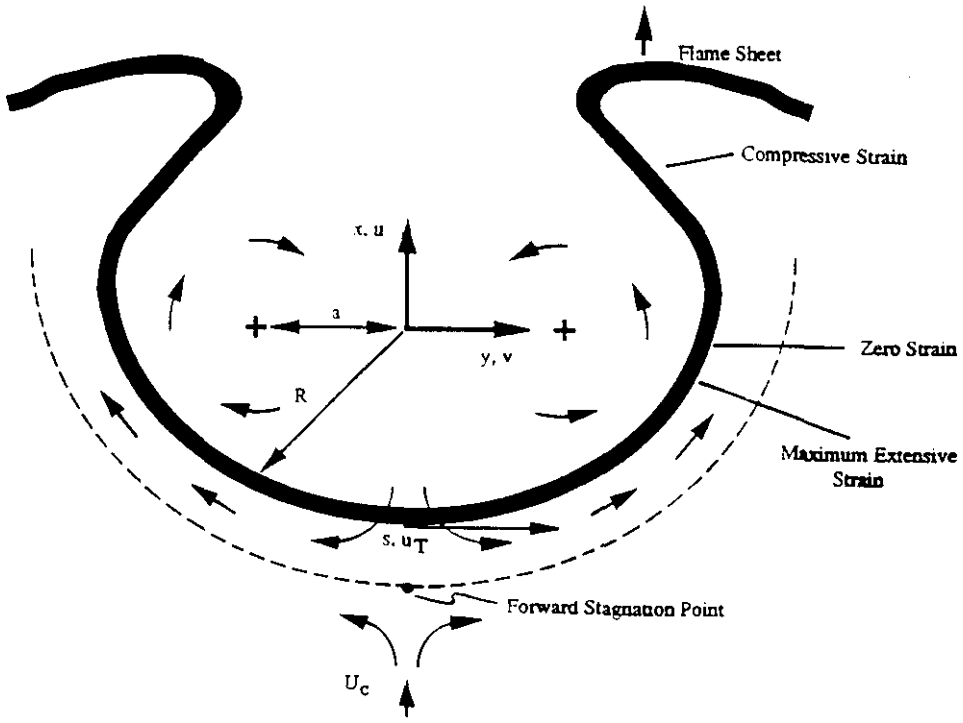

(a)

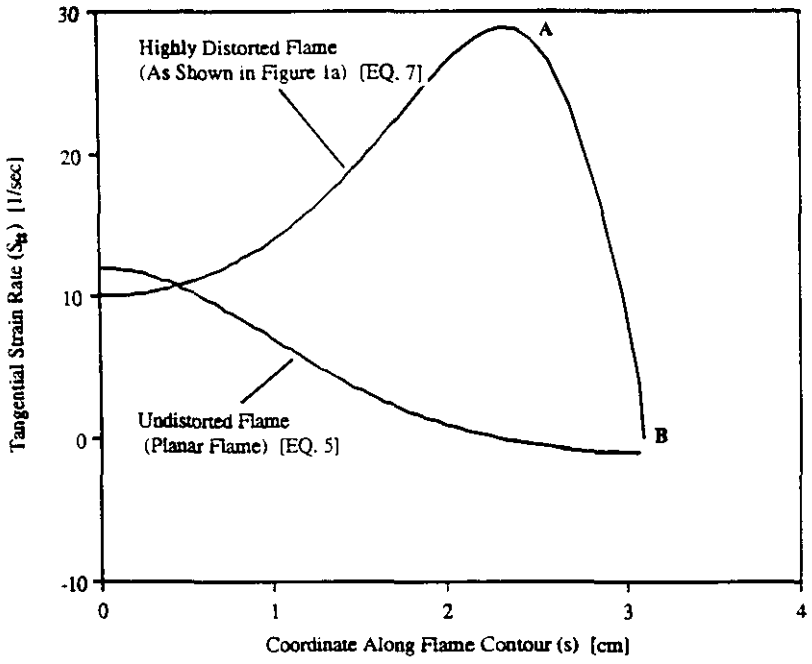

(b)

Figure 1. (a) Schematic of the Velocity Field for a Flame-Vortex Interaction., (b) Theoretical Tangential Strain Rate Profiles for a Flame-Vortex Interaction

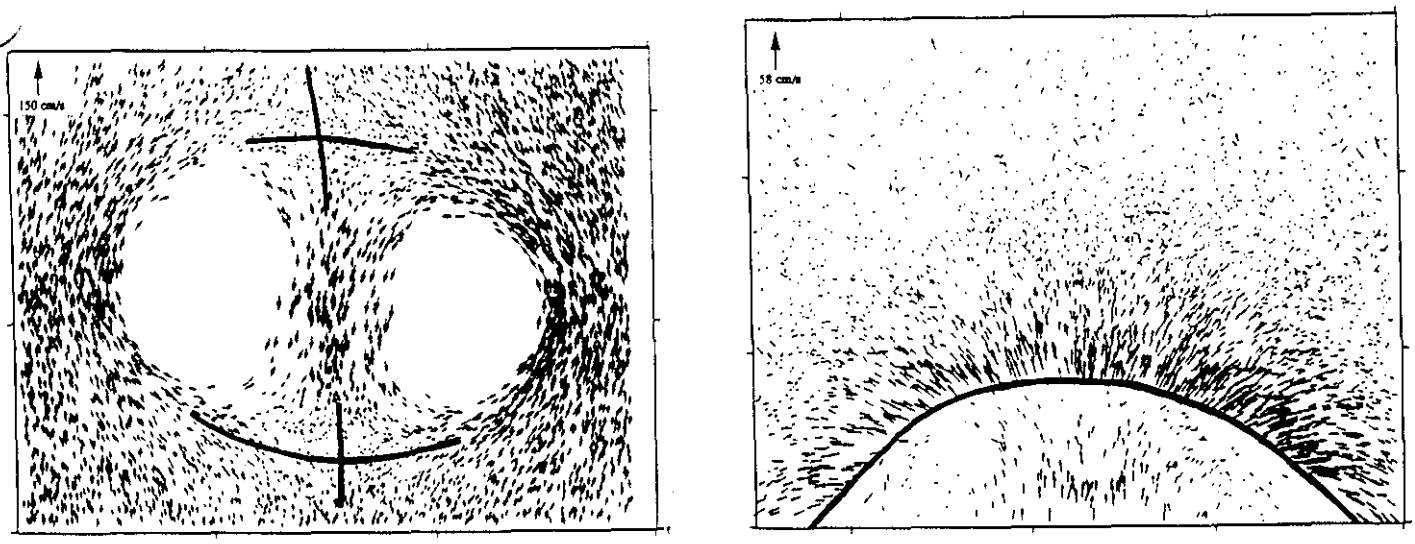

(a) (b)

Figure 2. Velocity Field Images for (a) Vortex Only (In Vortex Frame of Reference), maximum rotational velocity U_θ=107 cm/s, distance between vortex centers D=3.8 cm, (b) Flame Only (In Lab Frame), burning velocity S_L=7.5 cm/s. Field of view for each image is approximately 8 cm wide by 6 cm high .

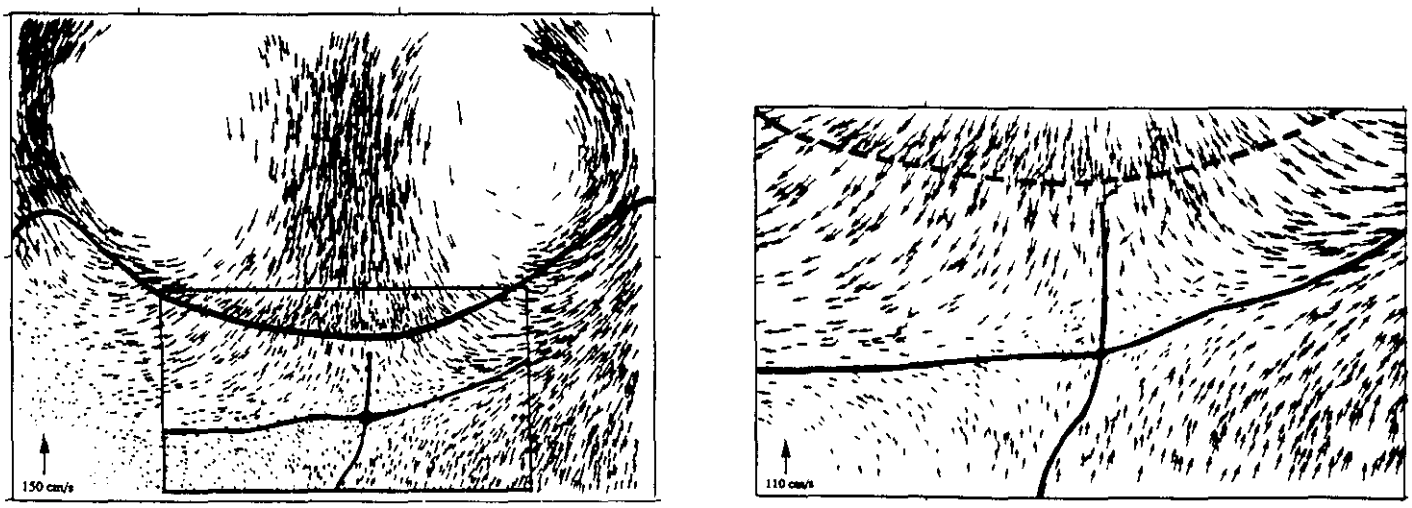

(a) (b)

Figure 3. (a) Velocity Field Image of Intermediate Phase of Flame-Vortex Interaction (In Vortex Frame of Reference, t= 26 ms), (b) Magnified View of the Intermediate Phase Forward Stagnation Point.

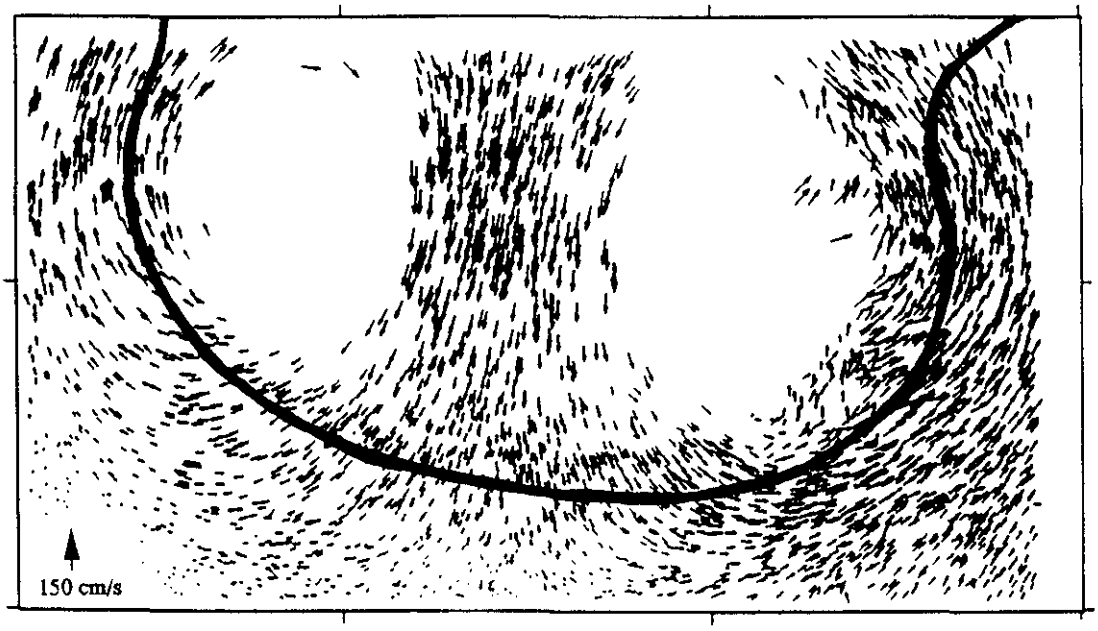

Figure 4. Velocity Field Image of the Late Phase of the Flame-Vortex Interaction (In Vortex Frame of Reference, t= 34 ms).

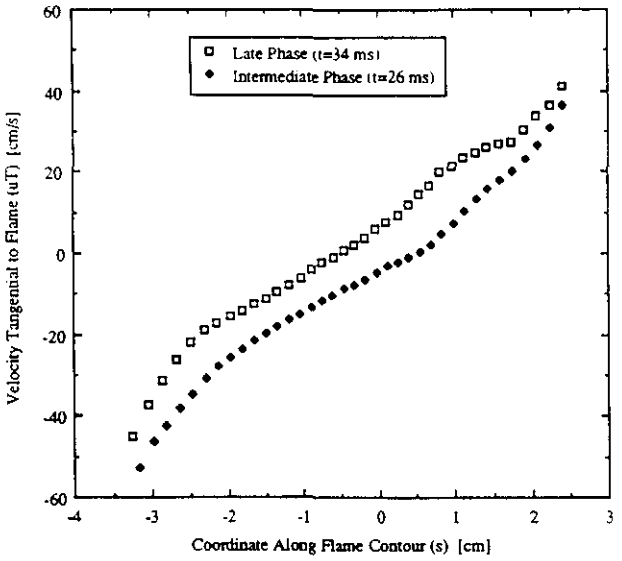

Figure 5. Velocity Tangential to Flame Contour for Intermediate Phase and Late Phase of Flame-Vortex Interaction.

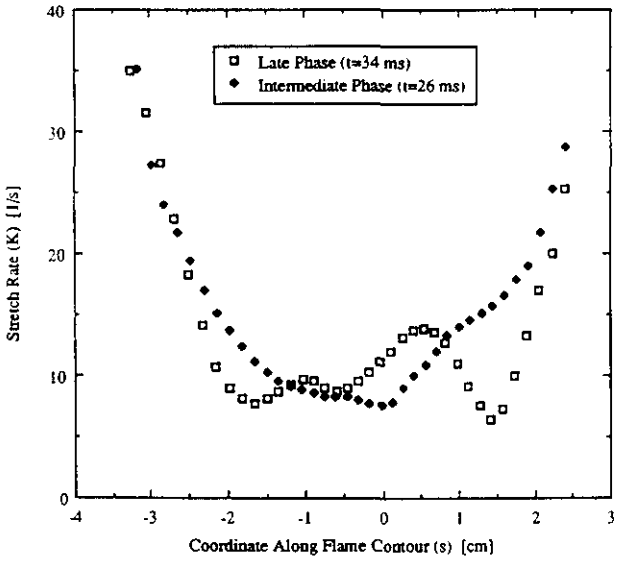

Figure 6. Measured Stretch Rate (K) Obtained by Applying Equation 1 to PIV Velocity Data.

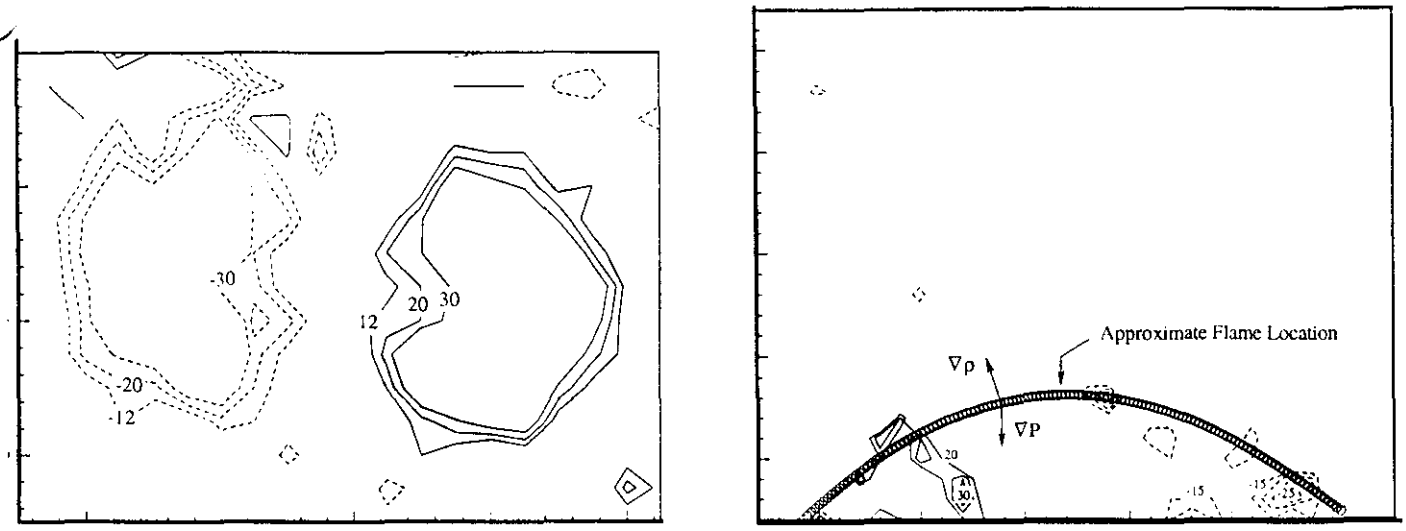

(a) (b)

Figure 7. Contours of Vorticity (ω_z) Measured for (a) Vortex Only Case, (b) Flame Only Case. Units are sec^{-1}

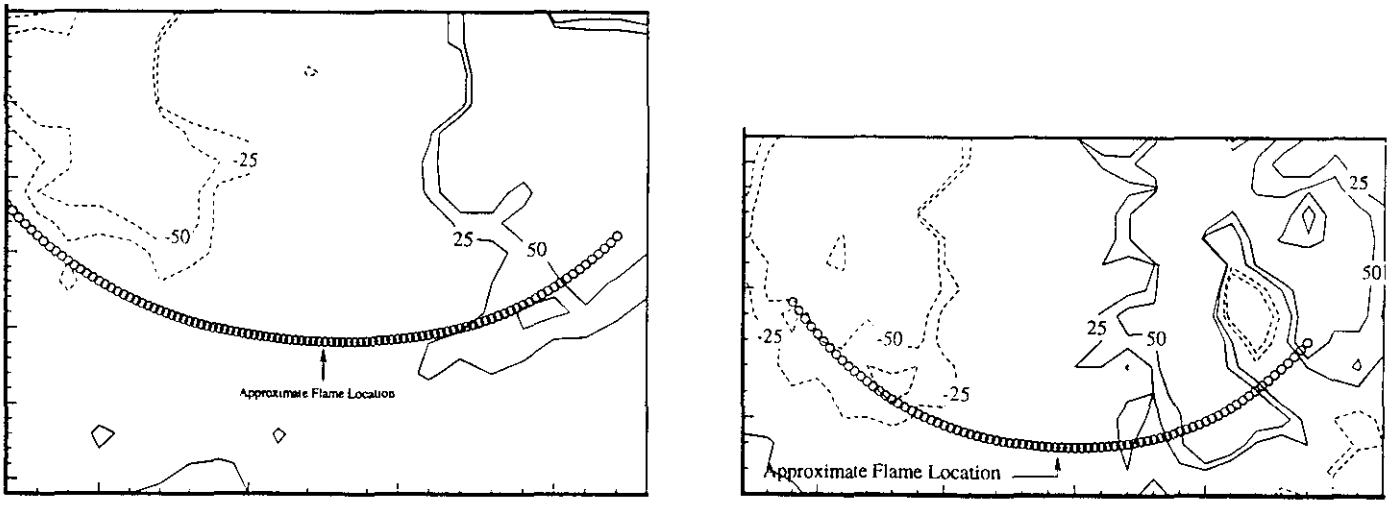

(a) (b)

Figure 8. Vorticity Contours for (a) Intermediate Phase, t= 26 ms and (b) Late Phase, t= 34 ms of Flame-Vortex Interaction. Units are sec^{-1}.

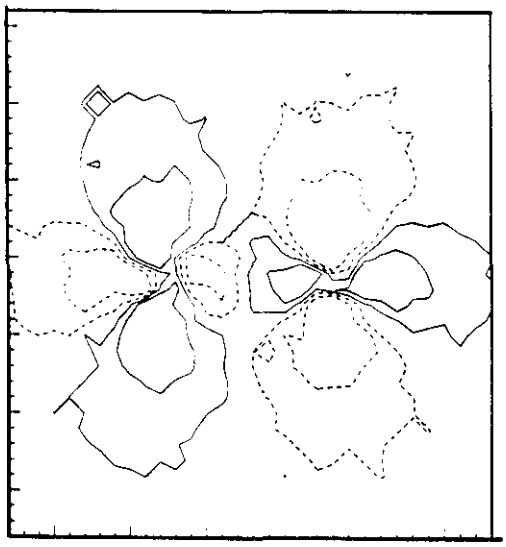

(a)

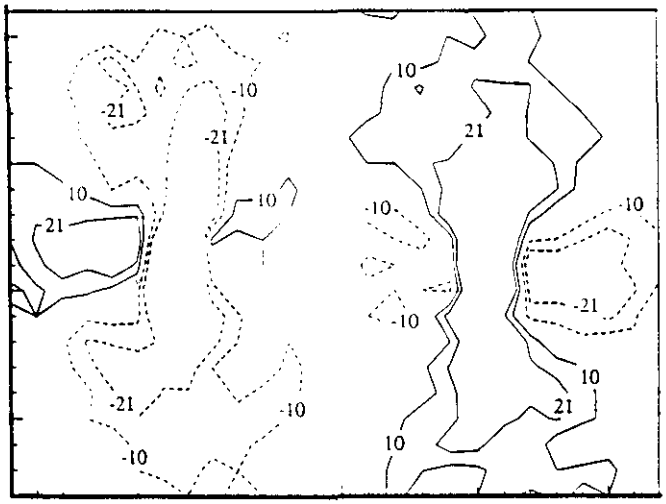

(b)

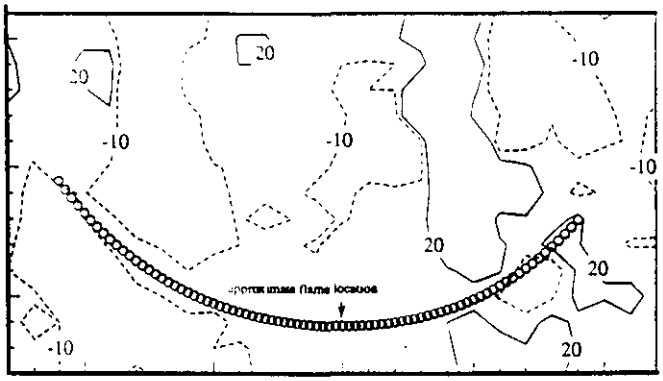

(c)

Figure 9. Shear Strain Rate (S_{xy}), (a) Theoretical Example, (b) Vortex Only, (c) Late Phase of Flame-Vortex Interaction, t= 34 ms.